SUBMITTED ON DECEMBER 14, 2023
Preprint typeset using LaTeX style emulateapj v. 12/16/11

RESTORATION OF THE TULLY-FISHER RELATION BY STATISTICAL RECTIFICATION

HAI FU
Department of Physics & Astronomy, University of Iowa, Iowa City, IA 52242
submitted on December 14, 2023

ABSTRACT

I employ the Lucy (1974) rectification algorithm to recover the inclination-corrected distribution of local disk galaxies in the plane of absolute magnitude and H I velocity width. By considering the inclination angle as a random variable with a known probability distribution, the novel approach eliminates the need for individual galaxy inclination-angle estimation (e.g., from axial ratio) and leverages the statistical strength derived from the entire sample of 28,264 H I-selected disk galaxies in the Arecibo Legacy Fast ALFA (ALFALFA) survey. I show that the restored distribution of *edge-on* H I velocity width and *face-on i*-band absolute magnitude follows a single Tully-Fisher relation, $M_i = M_0 - 2.5\beta\ [\log(W_{20,\rm HI}/250{\rm km/s})]$, with $M_0 = -19.77 \pm 0.04$, $\beta = 4.1 \pm 0.3$ between $-22 \lesssim M_i \lesssim -14$. Since the method accounts for measurement errors, the intrinsic dispersions of the relation are directly measured: $\sigma(\log W_{20}) \approx 0.066$ dex and $\sigma(M_i) \approx 0.52$ mag. The potential of this statistical rectification technique is considerable. Beyond its application to the Tully-Fisher relation, it also facilitates investigations into edge-on velocity-width function, face-on luminosity function, edge-on thickness, and face-on ellipticity of disk galaxies. Additionally, the technique can be effectively utilized in high-redshift galaxy samples with restricted spatial resolution.

Subject headings: Astrostatistics, Scaling relations, Disk galaxies, Galaxy rotation, Galaxy luminosities

1. INTRODUCTION

In observational astronomy, a prevalent challenge involves recovering intrinsic properties from observed ones. This restoration is essential due to the potential alteration of intrinsic properties by factors like viewing angles, dust extinction, atmospheric seeing, instrumental point spread function (PSF), as well as statistical and instrumental noise. In general, the transformation from the intrinsic probability distribution to the observed one follows the *law of total probability*, which for two-dimensional problems is:

$$\phi(x,y) = \iint \psi(\xi,\eta) P(x,y|\xi,\eta) d\xi d\eta, \tag{1}$$

where (ξ,η) are the intrinsic properties, (x,y) the observed properties, $\psi(\xi,\eta)$ the probability density function (PDF; or distribution in short) of the intrinsic properties, $\phi(x,y)$ the PDF of the observed properties, and $P(x,y|\xi,\eta)$ the conditional PDF. The definition of the conditional PDF is that $P(x,y|\xi,\eta)dxdy$ is the probability that x' and y' respectively fall in the interval $(x,x+dx)$ and $(y,y+dy)$ when $\xi' = \xi$ and $\eta' = \eta$. The objective is to reverse this equation to restore $\psi(\xi,\eta)$ from $\phi(x,y)$ given the knowledge of $P(x,y|\xi,\eta)$.

Convolution is a special case of Eq. 1 when the conditional PDF can be expressed as a function of the differences between intrinsic and observed properties:

$$\phi(x,y) = \iint \psi(\xi,\eta) K(x-\xi, y-\eta) d\xi d\eta, \tag{2}$$

where $K(x-\xi, y-\eta)$ is called the convolution kernel, and its shape is invariant across the plane of ξ and η. Similar to the general reversal problem, the goal of *deconvolution* is to recover $\psi(\xi,\eta)$ from $\phi(x,y)$ given the knowledge of $K(x-\xi, y-\eta)$. One particularly important problem is "image restoration", that is to recover the intrinsic surface brightness map by removing or reducing of the effects of atmospheric seeing and/or instrumental PSF due to telescope/interferometer geometry. Popular *deconvolution* algorithms include RICHARDSON-LUCY (Richardson 1972; Lucy 1974), CLEAN (Högbom 1974; Cornwell 2009), and WIENER-HUNT (Orieux et al. 2010).

Because the conditional PDF in Eq. 1 generally varies in the plane of ξ and η, the aforementioned deconvolution algorithms cannot handle the reversal of the law of total probability except one algorithm. The iterative rectification algorithm of Lucy (1974) is in fact *designed* to reverse Eq. 1, and that is the main difference between the Lucy (1974) rectification algorithm and the Richardson (1972) deconvolution algorithm.

In this work, I will employ the Lucy (1974) rectification algorithm to restore the Tully-Fisher relation (Tully & Fisher 1977), which is an important scaling relation between rotation velocity and luminosity of disk galaxies. In numerous previous studies of the relation (e.g., Tully & Courtois 2012; Zaritsky et al. 2014; Tiley et al. 2016; Desmond 2017; Übler et al. 2017; Topal et al. 2018; Ball et al. 2023), the observed luminosities and velocity widths were corrected using inclination angles estimated from the observed axial ratios (b/a). The rectification technique implemented here eliminates the need of b/a measurements and replaces the highly uncertain individual correction with robust statistical rectification. First, I briefly introduce the rectification algorithm in §2. Next in §3, I describe the survey data set (§3.1), construct the joint PDF (§3.2), restore the intrinsic distribution (§3.3), and compare the resulting Tully-Fisher relation with that from the b/a-based individual correction method (§3.4). Finally, I summarize the work and comment on future applications of the technique in §4.

2. ALGORITHM

For simplicity, I first derive the equations of the algorithm in one dimension (1D), then provide the equivalent iterative equations for two-dimensional (2D) problems.

The iterative rectification algorithm of Lucy (1974) is constructed using Bayes' theorem. Given the law of total probability, $\phi(x) = \int \psi(\xi) P(x|\xi) d\xi$, one can define its inverse inte-

gral, $\psi(\xi) = \int \phi(x) Q(\xi|x) dx$, with the inverse conditional PDF $Q(\xi|x)$. In other words, given that $P(x|\xi)dx$ is the probability that x' falls in the interval $(x, x+dx)$ under the condition that $\xi' = \xi$, $Q(\xi|x)d\xi$ is the probability that ξ' falls in the interval $(\xi, \xi+d\xi)$ under the condition that $x' = x$. With Bayes' theorem, $\phi(x)Q(\xi|x) = \psi(\xi)P(x|\xi)$, one can replace $Q(\xi|x)$ in the inverse integral and obtain the following equation:

$$\begin{aligned}\psi(\xi) &= \int \phi(x) Q(\xi|x) dx \\ &= \int \phi(x) \Big(\frac{\psi(\xi) P(x|\xi)}{\phi(x)} \Big) dx \\ &= \psi(\xi) \int \frac{\phi(x)}{\phi(x)} P(x|\xi) dx \end{aligned} \tag{3}$$

At first glance, the above may seem to be trivial as the terms cancel out and the integral of $P(x|\xi)$ must be unity by definition. But it inspired a highly efficient algorithm that allows the iterative solution of the intrinsic distribution function $\psi(\xi)$ from the observed distribution function $\phi(x)$, when the conditional PDF $P(x|\xi)$ is known. At the r-th iteration, the Lucy (1974) algorithm is simply described by two iterative equations:

$$\phi^r(x) = \int \psi^r(\xi) P(x|\xi) d\xi \tag{4}$$

$$\psi^{r+1}(\xi) = \psi^r(\xi) \int \frac{\tilde{\phi}(x)}{\phi^r(x)} P(x|\xi) dx \tag{5}$$

Evidently, Eq. 4 is the law of total probability, and Eq. 5 is the iterative version of the Bayes identity in Eq. 3. For two-dimensional problems incorporating measurement errors (σ_x, σ_y), the iterative equations become:

$$\phi^r(\tilde{x}, \tilde{y}) = \iint \psi^r(\xi, \eta) P(\tilde{x}, \tilde{y}|\xi, \eta, \sigma_x, \sigma_y) d\xi d\eta \tag{6}$$

$$\psi^{r+1}(\xi, \eta) = \psi^r(\xi, \eta) \iint \frac{\tilde{\phi}(\tilde{x}, \tilde{y})}{\phi^r(\tilde{x}, \tilde{y})} P(\tilde{x}, \tilde{y}|\xi, \eta, \sigma_x, \sigma_y) d\tilde{x} d\tilde{y} \tag{7}$$

In Eqs. 5 & 7, the key input is $\tilde{\phi}$, which is the observed distribution function of the observables. The tilde hat is used to distinguish it from the true distribution function, which is denoted simply as ϕ. Similarly, I have used $(\tilde{x}, \tilde{y})$ to denote the measured values (i.e., with errors) and (x, y) to denote the true values (i.e., without errors).

Given the iterative equations, the procedure to carry out the iterative algorithm is to:

1. quantify the observed distribution function $\tilde{\phi}(\tilde{x}, \tilde{y})$ from the data,
2. define the conditional PDF $P(\tilde{x}, \tilde{y}|\xi, \eta, \sigma_x, \sigma_y)$ for the particular problem,
3. prescribe an initial guess of the intrinsic distribution function $\psi^0(\xi, \eta)$, and
4. solve iteratively for the intrinsic distribution function $\psi(\xi, \eta)$ with the previous two equations.

3. APPLICATION TO THE TULLY-FISHER RELATION

In this section, I apply the iterative rectification technique to restore the Tully-Fisher relation from the observed distribution of Arecibo H I-selected galaxies. A Python notebook of the full analysis is made publicly available[1]. I define $\tilde{x}$ as the observed projected velocity width (W_{20} in §3.1), ξ the edge-on velocity width, $\tilde{y}$ the observed projected i-band absolute magnitude (M_i in §3.1), and η the face-on i-band absolute magnitude. The goal is to recover the distribution of the galaxy sample in ξ and η, $\psi(\xi, \eta)$, from the observed distribution in $\tilde{x}$ and $\tilde{y}$, $\tilde{\phi}(\tilde{x}, \tilde{y})$. As in the previous section, x and y are reserved for true projected velocity width and true projected i-band absolute magnitude in the absence of measurement errors, and they will be integrated out when evaluating the joint PDF of $\tilde{x}$ and $\tilde{y}$.

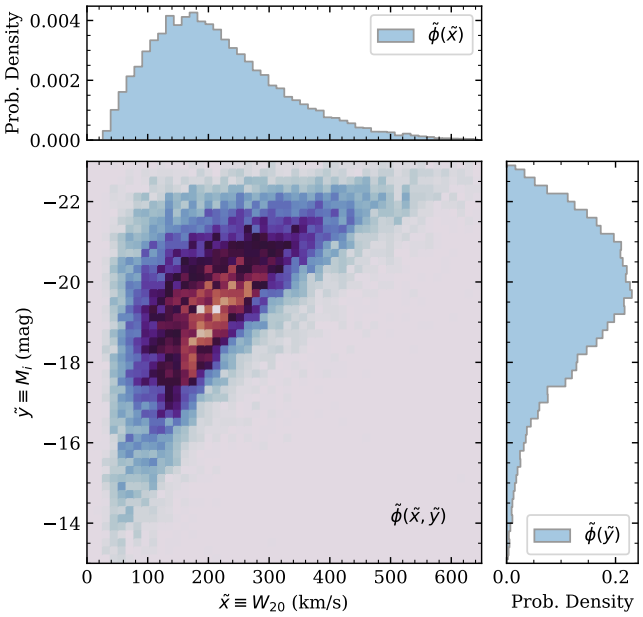

FIG. 1.— The distribution of ALFALFA-SDSS galaxies in the plane of i-band absolute magnitude vs. H I line width. This is the input $\tilde{\phi}(\tilde{x}, \tilde{y})$ function, which will be rectified by the Lucy algorithm to *statistically* remove the effects from random disk orientations and random measurement errors. Here and in most of the subsequent figures, the main panel shows the 2D distribution, and the side panels show the marginalized distributions over each axis.

3.1. *Data*

The H I measurements are taken from the 100% complete ALFALFA catalog (the $\alpha.100$ sample; Haynes et al. 2018) and the absolute magnitudes are from the cross-matched ALFALFA-SDSS galaxy catalog (Durbala et al. 2020). In both catalogs, distances to the galaxies are inferred from Hubble's law with $H_0 = 70$ km s^{-1} Mpc^{-1} and a local peculiar velocity model (for details, see §3 of Haynes et al. 2018). I merge the two catalogs based on the Arecibo General Catalog (AGC) ID, resulting in a total of 31,500 entries with 53 columns. A total of 28,264 sources (90% of the $\alpha.100$ sample) in the merged catalog have valid velocity widths and absolute magnitudes, and that forms the galaxy sample for this study, because no further down-selection is necessary. The sample is at low redshift ($z < 0.06$) and covers a wide range in i-band absolute magnitude ($-13 < M_i < -23$).

For the H I velocity width, I start with the reported velocity width at 20% level of each of the two peaks in the line profile (Column `W20`), because it is expected to capture more of the flat parts of a rotation curve than the 50% level velocity

[1] https://github.com/fuhaiastro/TFR_Lucy_Algorithm

width (W50). All reported velocity widths are corrected for instrumental broadening following the simulations of Springob et al. (2005). W20 are given in observed frame instead of in rest frame, and the rest-frame H I velocity widths (W_{20}) are obtained by dividing W20 by $(1+cz_\odot/c)$, where $cz_\odot$ is the Heliocentric velocity of the H I profile (column Vhelio in the catalog).

For the i-band absolute magnitude, I start with the extinction corrected i-band absolute magnitude (Column ABSMAG_I_CORR). It is derived from SDSS i-band cmodel magnitude and has been corrected for both foreground Galactic extinction and internal dust extinction due to inclination. For the internal correction, the authors used the r-band axial ratio (b/a) from SDSS exponential model fits (expAB_r) and a simple logarithmic formula for the additional dust extinction due to inclination, $M_{i,\rm corr} = M_i + \gamma_i(M_i)\log(b/a)$. Because magnitudes uncorrected for inclination is desired for this study, I reversed the internal extinction correction using the listed γ_i values in the catalog (gamma_i) and the relation the authors used to calculate γ_i from M_i: $\gamma_i = -0.15M_i - 2.55$ for $M_i < -17$. For less luminous galaxies with $M_i > -17$, M_i equals $M_{i,\rm corr}$ since $\gamma_i = 0$. After this process, the resulting M_i magnitudes are corrected for foreground Galactic extinction only.

Lastly, the uncertainties of the measurements are needed to construct the joint conditional PDF in Eq. 6 & 7. The mean uncertainty of W50 in the catalog is 18 km s^{-1}, which is comparable to the spectral resolution of ALFA (10 km s^{-1} after Hanning smoothing, for a channel spacing of 5 km s^{-1}). The uncertainty of W20 is not reported because they are difficult to quantify for the adopted polynomial fitting algorithm, so I assume a conservative uncertainty of 20 km s^{-1} for W_{20}. For the absolute magnitude M_i, I adopt the mean of the magnitude errors listed in ABSMAG_I_CORR_ERR, which is 0.14 mag.

Figure 1 shows the distribution of the sample in the plane of W_{20} and M_i. This 2D histogram represents $\tilde{\phi}(\tilde{x},\tilde{y})$ in Eq. 7.

3.2. *Conditional Probability Density Function*

Both the H I velocity width and the absolute magnitudes are affected by the inclination angle. The true projected values and the intrinsic values follow these simple relations:

$$x = \sqrt{(\xi \sin i)^2 + \sigma_0^2} \tag{8}$$

$$y = \eta - \gamma \log(\cos i) \tag{9}$$

where the inclination angle i is defined to be 0° when viewed face-on and 90° when viewed edge-on.

In Eq. 8, the projected velocity width is expressed as the quadrature sum of the line-of-sight projection of the edge-on velocity width and the velocity width from random motions (σ_0). I set $\sigma_0 = 30$ km s^{-1} based on the lower boundary in the observed distribution of velocity widths shown in Figure 1.

In Eq. 9, the projected absolute magnitude follows the parameterization in Eq. 27 of Giovanelli et al. (1994), which fits well the observed inclination dependency of M^* (the knee of the optical luminosity function) for low-z disk galaxies in the five SDSS filters (Shao et al. 2007). Obviously, the extinction coefficient γ depends on wavelength. Here I set $\gamma = 0.73$ using the result of Shao et al. (2007) for the SDSS i-band (γ_2 in their Table 4). To understand the physical meaning of γ, one can compare the extinction term above, $A = \gamma \log(\sec i)$, with the plane-parallel extinction, $A' = 2.5\log(e)\tau_0(\sec i - 1)$, where τ_0 is the face-on optical depth of the disk. At the face-on limit

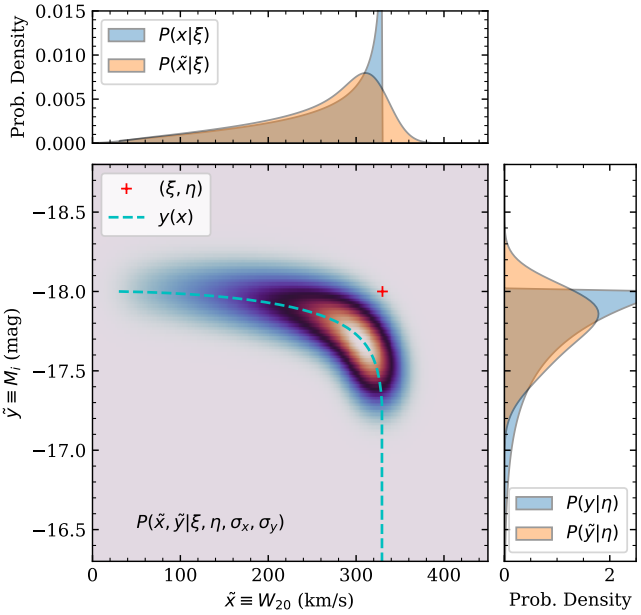

FIG. 2.— The joint PDF $P(\tilde{x},\tilde{y}|\xi,\eta,\sigma_x,\sigma_y)$ for $\xi = 330$ km s^{-1}, $\eta = -18$, $\sigma_x = 20$ km s^{-1}, $\sigma_y = 0.14$, $\sigma_0 = 30$ km s^{-1}, and $\gamma = 0.73$. The intrinsic values are indicated by the *red cross*, which is offset from the peak of the PDF. The top panel shows the PDF marginalized over the $\tilde{y}$-axis (*yellow*). This gives the PDF of the measured values, $P(\tilde{x}|\xi,\sigma_x)$ per Eq. 13, which can be compared with the PDF of the true projected values $P(x|\xi)$ from Eq. 10 (*blue*) to see the effects of measurement errors. The right panel shows the joint PDF marginalized over the $\tilde{x}$-axis and $P(y|\eta)$ from Eq. 11.

($i \to 0$), $A \to \gamma \log(e)(\sec i - 1)$, one sees that $\gamma = 2.5\tau_0$. So $\gamma = 0.73$ implies an face-on optical depth of $\tau_0 = 0.29$, and disks become optically thick when $\gamma > 2.5$.

Assuming the disks are randomly oriented on the sky, the PDF of the inclination angle is $P(i) = \sin i$. Given this and the relations in Eqs. 8-9, the conditional PDF of x and y are:

$$P(x|\xi) = \frac{x/\xi}{\sqrt{\xi^2 - (x^2 - \sigma_0^2)}} \text{ when } 0 \le x \le \xi \tag{10}$$

$$P(y|\eta) = \frac{\ln 10}{\gamma} 10^{(\eta - y)/\gamma} \text{ when } \eta < y \tag{11}$$

In addition, since both x and y are related to the same inclination angle i, the two are correlated:

$$y = \eta - 0.5\gamma \log\left(1 - \frac{x^2 - \sigma_0^2}{\xi^2}\right) \tag{12}$$

The joint conditional PDF of x and y is determined by Eqs. 10-12 because when integrated over one axis it must recover the conditional PDF of the other axis:

$$\int P(x,y|\xi,\eta)dy = P(x|\xi) = \frac{x/\xi}{\sqrt{\xi^2 - (x^2 - \sigma_0^2)}} \tag{13}$$

$$\int P(x,y|\xi,\eta)dx = P(y|\eta) = \frac{\ln 10}{\gamma} 10^{(\eta - y)/\gamma} \tag{14}$$

The correlation relation in Eq. 12 explains why η drops off after the integral over y in Eq. 13 and ξ drops off in Eq. 14: Eq. 12 allows η or ξ to be expressed by the other three parameters.

All measurements have errors, and the errors scatter the measured value around the true value following a PDF that is

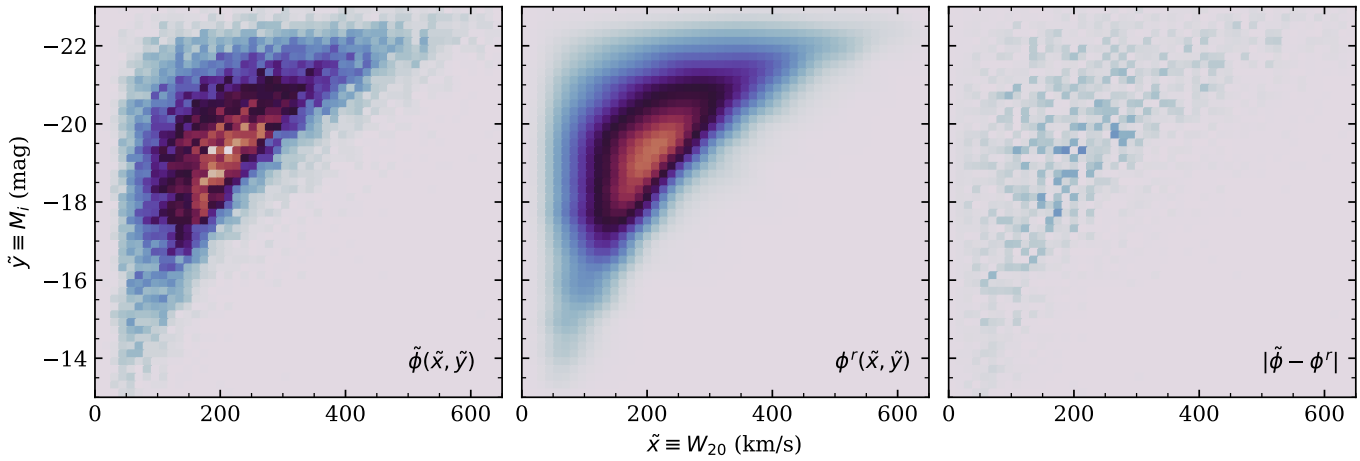

FIG. 3.— Data vs. model. From left to right are respectively the observed $\tilde{\phi}$ distribution (same as Fig. 1), the model ϕ^r distribution after 30 iterations, and the absolute differences between the two distributions. For fair comparison, the same color scale and contrast are used in all panels.

usually assumed to be Gaussian. Because the velocity widths and the absolute magnitudes come from two different surveys (ALFALFA and SDSS), and only the latter depends on the distance to the source, we can safely assume that the measurement errors in x and y are uncorrelated. As a result, the error PDF is a 2D Gaussian with major and minor axes aligned with the x and y axes:

$$G(x-\tilde{x},y-\tilde{y}|\sigma_x,\sigma_y)=\frac{1}{2\pi\sigma_x\sigma_y}\exp\left(-\frac{(\tilde{x}-x)^2}{2\sigma_x^2}\right)\exp\left(-\frac{(\tilde{y}-y)^2}{2\sigma_y^2}\right) \quad (15)$$

And the joint conditional PDF of $\tilde{x}$ and $\tilde{y}$ is then $P(x,y|\xi,\eta)$ convolved with the 2D Gaussian:

$$P(\tilde{x},\tilde{y}|\xi,\eta,\sigma_x,\sigma_y)=\iint P(x,y|\xi,\eta)G(x-\tilde{x},y-\tilde{y}|\sigma_x,\sigma_y)dxdy \quad (16)$$

Efficient convolution algorithms based on Fast Fourier Transform (FFT) can be used to evaluate $P(\tilde{x},\tilde{y}|\xi,\eta,\sigma_x,\sigma_y)$ on the $(\tilde{x},\tilde{y})$ plane for a grid of (ξ,η). Over the parameter ranges covered by the data, $0<x<650\,\mathrm{km\ s^{-1}}$ and $-23<y<-13$, I calculate the joint PDF on a 51×51 grid in both $(\tilde{x},\tilde{y})$ and (ξ,η) with spacings of $13\,\mathrm{km\ s^{-1}}$ and 0.2 mag. The resulting 4D array can be interpolated and used for integrations in the iterative process (Eqs. 6 and 7).

Figure 2 shows an example of the joint PDF. As expected, the population is dominated by more inclined disks, which show higher velocity widths but suffer more internal dust extinction. The correlation between $\tilde{x}$ and $\tilde{y}$ in Eq. 12 is also evident in the plot. As described in §3.1, I estimated the mean measurement errors to be $\sigma_x=20\,\mathrm{km\ s^{-1}}$ and $\sigma_y=0.14$ mag. Note that an accurate knowledge of the measurement errors is important to quantify the intrinsic dispersion of the restored intrinsic relation, because if the errors were underestimated (overestimated), the recovered intrinsic distribution would have shown a larger (smaller) scatter.

3.3. *Rectified Intrinsic Distribution*

To start the iterative process, one needs to prescribe an initial distribution for $\psi(\xi,\eta)$. Usually it is recommended to prescribe the observed distribution as the initial guess, $\psi^0(\xi,\eta)=\tilde{\phi}(\tilde{x},\tilde{y})$, to speed up the convergence. But because the position of the intrinsic position is offset from the peak of the joint PDF, as illustrated in Figure 2, one would expect similar offsets between ψ and ϕ. So I simply prescribed a flat distribution as the initial guess, $\psi^0(\xi,\eta)=$ constant, over the parameter ranges covered by the data.

At the end of each iteration, both the rectified distribution $\psi^r(\xi,\eta)$ (Eq. 7) and its corresponding projected distribution $\phi^r(\tilde{x},\tilde{y})$ (Eq. 6) are produced. The latter can be directly compared with the observed distribution $\tilde{\phi}(\tilde{x},\tilde{y})$ to assess the improvement of the model after each iteration. As already noted in previous works, the Lucy algorithm is very efficient. After just a few iterations, a narrow curved distribution begins to emerge in ψ^r and the resulting ϕ^r starts to converge onto the input $\tilde{\phi}$. Based on the residual map $(\tilde{\phi}-\phi^r)$ and the expected Poisson noise of $\tilde{\phi}$, I find that the reduced χ^2_ν decreases from 13.7 after the first iteration to 1.0 after 30 iterations, which is a natural point to stop. Figure 3 shows that the model distribution of the observables accurately reproduces the observed distribution, and there is only statistical noise left in the residual map. The following results are all based on the products after 30 iterations.

Figure 4 shows the rectified distribution. The main panel shows that $\psi^r(\xi,\eta)$ is confined to a narrow, continuous sequence along the diagonal direction, revealing a tight correlation between the *edge-on* H I line width and the *face-on* i-band absolute magnitude of H I-selected galaxies. This is the i-band Tully-Fisher relation from the full sample of 28,264 H I-selected nearby ($z<0.06$) galaxies in the ALFALFA-SDSS catalog. Note that because the full sample is used (as opposed to selecting only high inclination disks as in previous studies), the absence of any significant secondary trend in the intrinsic distribution shows that the overwhelming majority of H I-selected galaxies follow a single Tully-Fisher relation.

The Tully-Fisher relation is usually parameterized as a power law between luminosity and velocity-width: $L\propto W^\beta$. Since magnitude is used here, the relation translates to $M_i=M_0-2.5\beta\,[\log(W/250\,\mathrm{km/s})]$, where β is the slope and M_0 is the intercept point at $250\,\mathrm{km\ s^{-1}}$. To determine these parameters, I fit the power-law relation to the ridge in the rectified distribution $\psi^r(\xi,\eta)$. First, I measure the width of the ridge and the location of its peak at each fixed $M_{i,\mathrm{face-on}}$ by fitting a Gaussian function to each row of the 2D distribution. Then, the same measurements are made at each fixed $W_{20,\mathrm{edge-on}}$ by

fitting each column. Finally, the power-law model is fit to the two sets of ridge peak measurements, using the Gaussian σ widths as relative errors. Similar M_0 values are found from both measurement sets, but the slopes differ: $\beta = 4.39 \pm 0.06$ and 3.78 ± 0.03 from by-row and by-column measurements, respectively. I take the mean of the two best-fit values and use their difference as an indicator of the uncertainty. The best-fit Tully-Fisher relation is:

$$M_{i,\mathrm{face-on}} = M_0 - 2.5\beta \log\left(\frac{W_{20,\mathrm{edge-on}}}{250\ \mathrm{km/s}}\right)$$
$$M_0 = -19.77 \pm 0.04$$
$$\beta = 4.1 \pm 0.3 \qquad (17)$$

Both the horizontal and the vertical widths of the ridge are roughly constant in logarithmic scales, with the median Gaussian σ values of $\sigma(\log W_{20}) = 0.066$ dex and $\sigma(M_i) = 0.52$ mag. These should be considered as the upper limits on the intrinsic dispersion of the Tully-Fisher relation, because there could be additional measurement errors that are not included in the joint PDF.

There are two important by-products from this exercise. Marginalized over each axis, the rectified distribution $\psi^r(\xi, \eta)$ provides the edge-on H I velocity-width function and the face-on i-band luminosity function of H I-selected disk galaxies. Of course, both functions remain uncorrected for the detection incompleteness and the luminosity-dependent volume incompleteness. Nevertheless, the effects of inclination correction is evident when comparing the histograms in the side panels of Fig. 4. The face-on luminosity function is simply shifted by $\sim$0.2 mag towards to brighter end. The changes in the velocity-width function are more pronounced. After the rectification, not only its peak shifts by $\sim$50 km s^{-1} to the higher end, but also its slopes on both sides of the peak become steeper.

3.4. *Comparison with conventional method*

Having successfully restored the Tully-Fisher relation through rectification, in this subsection I compare the results with those from the traditional method of b/a-based individual inclination correction. The procedure is straight-forward. First, one estimates $\sin i$ of each galaxy using the following equation from Hubble (1926):

$$\sin^2 i = \frac{1-(b/a)^2}{1-q_0^2} \qquad (18)$$

where q_0 is the *assumed* edge-on axial ratio of the disk. Next, one corrects the projection effects in both the observed velocity width and the observed absolute magnitude using the estimated inclination angle of each galaxy and the following relations (same as Eqs. 8 and 9):

$$W_{20,\mathrm{corr}} = \sqrt{W_{20}^2 - \sigma_0^2}/\sin i$$
$$M_{i,\mathrm{corr}} = M_i + \gamma \log(\cos i) \qquad (19)$$

Finally, one generates the 2D histogram using the inclination-corrected measurements.

For a fair comparison, I carry out the b/a-based inclination corrections to the same ALFALFA-SDSS sample. To estimate the inclination angles, I assume $q_0 = 0.15$ and adopt the r-band axial ratio from SDSS exponential model fits (Column `expAB_r`). When applying the corrections, I adopt $\sigma_0 = 30$ km s^{-1} and $\gamma = 0.73$ to be consistent with the rectification analysis. Fig. 5 shows the resulting distribution using the corrected velocity widths and absolute magnitudes. This figure should be directly compared with Fig. 4 to see the significant differences between the results from the two different

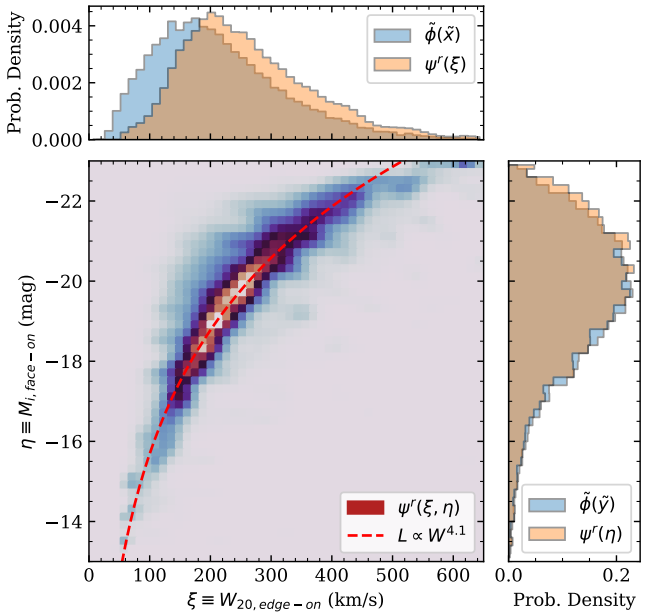

FIG. 4.— The rectified distribution $\psi^r(\xi, \eta)$ after 30 iterations. The red dashed curve in the main panel shows the best-fit Tully-Fisher relation in Eq. 17. The side panels compare the marginalized distributions before and after rectification (*blue* and *yellow*, respectively). They illustrates the differences between the observed H I-velocity width function and i-band luminosity function and the inclination angle corrected counterparts. Note that selection effects such as the magnitude limit and the volume incompleteness have not been corrected.

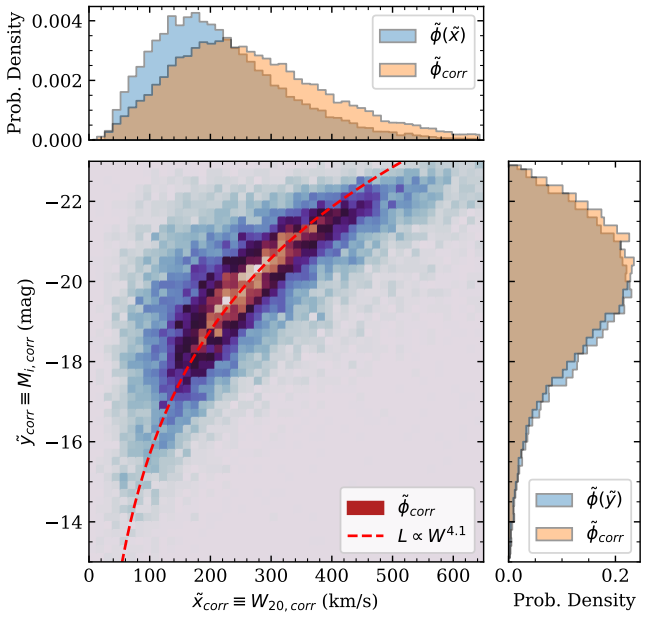

FIG. 5.— The distribution of the ALFALFA-SDSS galaxy sample after individual inclination angle correction based on the axial ratio (b/a). Same as in Fig. 4, the red dashed curve shows the Tully-Fisher relation in Eq. 17 and the side panels compare the marginalized distributions before and after the inclination-angle correction.

methods. There are substantial populations of "outlier" galaxies that seem to be either under-corrected or over-corrected in the traditional method. And probably due to these outliers, the corrected velocity-width function is significantly broader than that from the rectification method. The corrected Tully-Fisher relation also appears much broader than that from the rectification method.

The comparison between Fig. 4 and Fig. 5 clearly shows that superior results are obtained using the statistical rectification method. Now I briefly discuss why this is the case. When compared with the statistical rectification method, the main disadvantages of the traditional method include:

1. One additional measurement set, e.g., the axial ratio b/a, must be used to estimate $\sin i$;
2. The estimated inclination angle are not always reliable, introducing additional errors to the data;
3. Measurement errors of the observables are not corrected for.

The first item is particularly problematic at high redshifts when the angular sizes of galaxies are small compared to the spatial resolution. The latter two items make the resulting Tully-Fisher relation broader, which in turn makes it more difficult to quantify the intrinsic scatter of the relation.

Why the estimated inclination angles are unreliable? Eq. 18 was first derived by Hubble (1926), who assumed disk galaxies were axisymmetric oblate ellipsoids. One faces three main problems when using this equation to estimate the inclination angle:

1. The edge-on axial ratio, q_0, is not well determined and likely varies with morphological type and luminosity; the literature has assumed a range of values between $0.10 \leq q_0 \leq 0.25$ (e.g., Giovanelli et al. 1994; Xilouris et al. 1999; Übler et al. 2017).
2. Disk galaxies are not axisymmetric. Instead, they show median ellipticity between $0.07 \leq \epsilon \leq 0.18$ (e.g., Ryden 2006).
3. Axial ratios from different techniques differ (e.g., morphological fitting vs. isophotes) and are affected by observational conditions.

For these reasons, previous Tully-Fisher relation studies have excluded galaxies with low inclination angles to minimize the amount of correction to the velocity widths (e.g., $\sin i > 0.87$ when $i > 60°$). But this exclusion alone would severely reduce the sample size; e.g., the ALFALFA-SDSS galaxy sample would be reduced by a factor of three when I exclude galaxies with $i < 60°$. This exclusion not only reduces the statistical accuracy of the result, but also made it impossible to assess whether the excluded sample follows the same intrinsic correlation as the included sample.

4. SUMMARY AND FUTURE PROSPECT

The Tully-Fisher relation is an important empirical correlation between the edge-on rotation velocity and the face-on luminosity of disk galaxies. To determine this relation, three sets of observed properties are typically required: galaxy-integrated line widths (W), absolute magnitudes (M), and the axial ratios (b/a). The axial ratios are needed because the first two observed properties needed to be corrected for the inclination angle (i) of the disk. In this work, I have demonstrated a rectification technique that replaces *individual* inclination correction with *ensemble* statistical correction. It determines the Tully-Fisher relation with only two sets of observables (W and M) and utilizes the full sample of disk galaxies regardless of their inclination angles. The general philosophy of the method is as follows. When the observed properties can be converted from the intrinsic properties and the inclination angles with some known relations, one can predict joint PDF of the observed properties by assuming randomly oriented disks and random measurement errors. The recovery of the distribution of the intrinsic properties from the distribution of observables then becomes a reversal of *the law of total probability* in Eq. 1 that can be tackled numerically with the iterative rectification algorithm of Lucy (1974).

With 28,264 H I-detected disk galaxies from the ALFALFA-SDSS survey at $z < 0.06$, I show that the rectified distribution of *edge-on* H I line width and *face-on* i-band absolute magnitude of H I-selected disk galaxies follows a sharp power-law relation, $M_i = M_0 - 2.5\beta$ [$\log(W_{20,\rm HI}/250{\rm km/s})$], with $M_0 = -19.77 \pm 0.04$, $\beta = 4.1 \pm 0.3$. The intrinsic dispersions of the Tully-Fisher relation are $\sigma(\log W_{20}) \lesssim 0.066$ dex in velocity width and $\sigma(M_i) \lesssim 0.52$ mag in absolute magnitude. The absence of any significant secondary trends in the rectified distribution shows that all H I-selected disk galaxies follow a single Tully-Fisher relation. In addition, the rectified distribution marginalized over each axis provides the inclination-corrected H I velocity width function and the luminosity function of these galaxies, both of which show significant changes from the uncorrected distributions.

The statistical rectification technique can be applied to any observational problems where (1) the observed properties can be converted from the intrinsic properties by a relation that involves a "hidden" parameter (e.g., i) and (2) the PDF of the hidden parameter is precisely known. In future studies of disk galaxies, the technique can be used to determine not only the Tully-Fisher relation and the inclination-corrected luminosity function and velocity width function at high redshift (where no reliable axial ratio measurements are available), but also the edge-on thickness (q_0) and face-on ellipticity (ϵ) of low-redshift disk galaxies as a function of absolute magnitude (i.e., extending the work of Binney & de Vaucouleurs 1981; Vincent & Ryden 2005; Ryden 2006; Roychowdhury et al. 2010). The potential of the technique grows stronger with the increasing number of astronomical surveys generating statistical datasets encompassing large samples of galaxies.

The rectification technique would be less useful for small samples of galaxies, because the input distribution function $\tilde{\phi}$ is noisy. So for small samples, I recommend the Maximum Likelihood + Monte Carlo Markov Chain method implemented in our previous study (Isbell et al. 2018), where we used the observed CO line luminosities and velocity widths from small samples of galaxies to constrain the mean molecular gas fraction of galaxies between $0.01 < z < 3.26$. The Python notebook of that work is also publicly available[2].

I thank my colleagues Steve Spangler, Ken Gayley, and Kevin Hall for helpful conversations. This work is supported by the National Science Foundation (NSF) grant AST-2103251.

REFERENCES

Ball, C. J., Haynes, M. P., Jones, M. G., et al. 2023, ApJ, 950, 87
Binney, J., & de Vaucouleurs, G. 1981, MNRAS, 194, 679
Cornwell, T. J. 2009, A&A, 500, 65
Desmond, H. 2017, MNRAS, 472, L35
Durbala, A., Finn, R. A., Crone Odekon, M., et al. 2020, AJ, 160, 271
Giovanelli, R., Haynes, M. P., Salzer, J. J., et al. 1994, AJ, 107, 2036
Haynes, M. P., Giovanelli, R., Kent, B. R., et al. 2018, ApJ, 861, 49
Högbom, J. A. 1974, A&AS, 15, 417
Hubble, E. P. 1926, ApJ, 64, 321
Isbell, J., Deam, S., Reed, M., et al. 2018, in American Astronomical Society Meeting Abstracts, Vol. 231, American Astronomical Society Meeting Abstracts #231, #316.06
Lucy, L. B. 1974, AJ, 79, 745
Orieux, F., Giovannelli, J.-F., & Rodet, T. 2010, Journal of the Optical Society of America A, 27, 1593
Richardson, W. H. 1972, Journal of the Optical Society of America (1917-1983), 62, 55
Roychowdhury, S., Chengalur, J. N., Begum, A., & Karachentsev, I. D. 2010, MNRAS, 404, L60
Ryden, B. S. 2006, ApJ, 641, 773
Shao, Z., Xiao, Q., Shen, S., et al. 2007, ApJ, 659, 1159
Springob, C. M., Haynes, M. P., Giovanelli, R., & Kent, B. R. 2005, ApJS, 160, 149
Tiley, A. L., Bureau, M., Saintonge, A., et al. 2016, MNRAS, 461, 3494
Topal, S., Bureau, M., Tiley, A. L., Davis, T. A., & Torii, K. 2018, MNRAS, 479, 3319
Tully, R. B., & Courtois, H. M. 2012, ApJ, 749, 78
Tully, R. B., & Fisher, J. R. 1977, A&A, 54, 661
Übler, H., Förster Schreiber, N. M., Genzel, R., et al. 2017, ApJ, 842, 121
Vincent, R. A., & Ryden, B. S. 2005, ApJ, 623, 137
Xilouris, E. M., Byun, Y. I., Kylafis, N. D., Paleologou, E. V., & Papamastorakis, J. 1999, A&A, 344, 868
Zaritsky, D., Courtois, H., Muñoz-Mateos, J.-C., et al. 2014, AJ, 147, 134

[2] https://github.com/fuhaiastro/IXF18